Manipulation of molecular spin qudits with quantum circuits

Darío González[1,2], Guillem Aromí[3], Alicia Gómez[4], David Zueco[1,2], and Fernando Luis[1,2]
[1]*Instituto de Nanociencia y Materiales de Aragón, CSIC-University of Zaragoza, 50009 Zaragoza, Spain*
[2]*Departmento de Física de la Materia Condensada, Universidad de Zaragoza, 50009 Zaragoza, Spain*
[3]*Departamento de Química Inorgánica, Universidad de Barcelona, Barcelona, Spain and*
[4]*Centre of Astrobiology, INTA-CSIC, Madrid, Spain*

Superconducting circuits are known to provide a good platform to interact and manipulate molecular spin qudits. Here, we use them to characterize two different molecules, a PTMr organic free radical and a [DyLaDy] molecular trimer, in order to value their viability as a qubit and a qudit respectively, obtaining improvable results. Moreover, we perform pulse experiments that show the quality of our resonators, although we did not yet resolve the echo signal from the spin system.

I. INTRODUCTION: BACKGROUND AND MOTIVATION

One of the main goals in quantum technologies is building a quantum computer with enough power to perform large quantum simulations and quantum algorithms to support material research and solve current NP problems [1–3]. However, it should contain over thousands or millions of qubits, the basic logic units of this kind of computers, due to the complexity of the tasks and the need of quantum error correction (QEC) to protect quantum operations from noise [4].

Although there exist other possibilities, like Noisy Intermediate-Size Quantum devices (NISQs) [5] based on superconducting circuits [12] or on electron spins in semiconducting quantum dots [6] or atomic impurities [7], we here focus on spin systems in magnetic molecules [8], in particular in polynuclear complexes containing magnetic ions. These can include various electronic and nuclear spins, so they can realize multiple qubits or, in general, qudits of dimension $d > 2$ within each molecule. This opens the possibility of implementing small-scale algorithms, in particular QEC [9], so each molecule could be used as a logical qubit. In addition to this, they are characterized for having long coherence times T_2 [10] and good characteristics to integrate them in superconducting circuits [11].

The crucial challenge of this approach is how to build a computational architecture that allows performing basic operations on these molecular qudits and reading out the results [9]. At the same time, we have to ensure that spin coherence times remain sufficiently long to perform such operations. In order to address this challenge, we import techniques that are being currently used for other solid-state quantum computing platforms, in particular those developed for superconducting quantum processors [12]. Circuit Quantum Electro-Dynamics (QED) is based on coupling artificial atom-like systems (qubits in our case) to superconducting transmission lines and resonators in a chip. It provides a powerful platform for controlling, reading out and communicating different qubit realizations [13], in particular molecular spin qudits [14].

In this article, we explore the coupling between on-chip LC resonators and crystals of novel molecular spin qudits. We have chosen a [DyLaDy] molecular trimer, where each Dy encodes a qubit in its effective $S = 1/2$ ground state doublet. Thus, it represents a model two-qubit system: the local coordinations of the two Dy ions are slightly different, which makes their magnetic response also distinct and the two qubits separately addressable. Compared to previous [Dy_2] dimers [15], the insertion of the diamagnetic La ion reduces the qubit-qubit coupling to take the relevant transitions below 30 GHz. In addition to this, it provides a starting point for a three qubit system that can be obtained by replacing La with another magnetic ion. This is the smallest system for implementing QEC [16].

The coupling G_N of an ensemble of N spins to the resonator is a crucial parameter, since it determines if the spin states can be readout by detecting changes in the circuit resonances [12]. Because of that, measuring G_N is our first experimental goal. This also provides direct information on the spin Hamiltonian of a novel molecule hosting two coupled spin qubits. In order to understand the underlying physics, we first explore the spin-photon coupling in the case of model $S = 1/2$ free radical molecules and then describe our first experiments on [DyLaDy]. Finally, we describe our first attempts to exploit the circuit for controlling the spin states and measuring their spin coherence at very low temperatures.

II. METHODS

A. Experimental methods

Figure 1a shows the molecular structure of the [DyLaDy] trimer. The superconducting circuits used in these experiments contain several lumped-element resonators (LERs), but we only utilized one for each molecular sample. An image of the crystal deposited over this element, taken by the 'Servicio de Apoyo a la Investigación (SAI)' from the University of Zaragoza, is shown in Figure 1b. These circuits have been fabricated at the 'Centro de As-

trobiología' using maskless UV lithography.

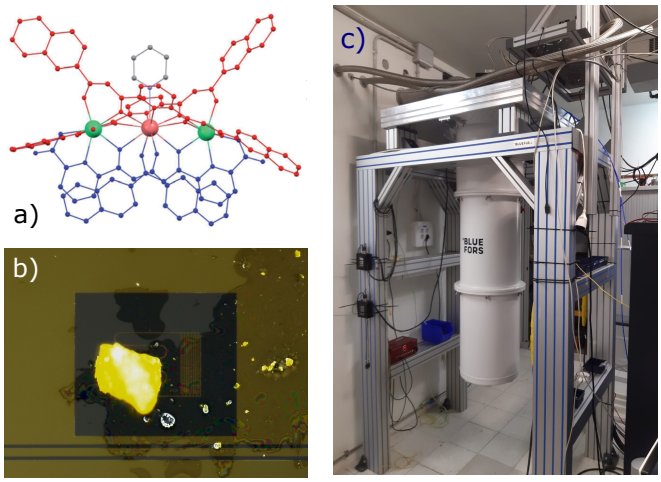

FIG. 1. a) Molecular structure of the [DyLaDy] trimer, where the green atoms are Dy ions and the red one is La. b) Optical microscopy image of the molecular crystal deposited over the superconducing circuit. c) Picture of the DR used in our experiments.

In order to observe the quantum phenomena analyzed in this article, it is necessary to reach very low temperatures ($\geq$ 10 mK) and apply quite strong magnetic fields ($\leq$ 1 T). These two requirements are fulfilled thanks to the *LD250* cryogen-free dilution refrigerator by Bluefors that hosts a superconducting vector magnet by American Magnetics (Fig. 1c). The signal transmitted through the device is delivered and picked-up via cryogenic semi-rigid coaxial wires. Input and output lines are connected to a Rohde & Schwarz *ZVB14* vector network analyser (VNA), which allows the characterization of electrical circuits by measuring their effect on the amplitude and phase of micro-wave (MW) signals.

Lastly, the study of the spin dynamics is feasible using a quantum control system (QCS), which is a direct digital conversion architecture for the generation and acquisition of arbitrarily shaped MW signals used to control and read out quantum devices. It enables designing and executing custom pulse sequences, all while automatically ensuring their synchronization down to sub-nanosecond levels. Our model is a Keysight *M9046A* high-power PXIe chasis. All the measurements have been automatised thanks to a control software managed by Python.

B. Theory methods

Albeit Dy^{3+} free lanthanide ions are characterized by a large angular momentum $J = 15/2$, its interaction with the crystal field created by its coordination shell in the molecule gives rise to a ground doublet that we can express with an effective spin $S = 1/2$. Thus, the simplest Hamiltonian that describes our two-spin system is given by [16]

$$\hat{\mathcal{H}}_S = \mu_B \vec{B}\tilde{g}_1\vec{S}_1 + \mu_B \vec{B}\tilde{g}_2\vec{S}_2 + \vec{S}_1\tilde{J}_{12}\vec{S}_2 \tag{1}$$

consisting of the electron Zeeman interaction of each ion $i = \{1, 2\}$ with the external magnetic field $\vec{B}$, characterized by the $\tilde{g}_i$ tensor, and the spin-spin interaction, mediated by the $\tilde{J}_{ij}$ tensor. For simplicity, we have neglected the hyperfine interaction of the Dy isotopes with $I_i \neq 0$. It is important to highlight the fact that the anisotropy generated by the metallic ion's environment is included in the main values of the $\tilde{g}_i$ tensor and that the $\tilde{J}_{ij}$ tensor does not introduce new degrees of freedom. Since it is mainly dominated by dipolar interactions, it can be calculated as $\tilde{J}_{ij} \simeq [\tilde{g}_i \cdot \tilde{g}_j - 3(\tilde{g}_i \cdot \hat{r}_{ij})(\hat{r}_{ij} \cdot \tilde{g}_j)]\,\mu_B^2/r_{ij}^3$.

If we now consider that our spins are coupled to a superconducting circuit, the total system is described by the Jaynes-Cummings Hamiltonian

$$\hat{\mathcal{H}}_T = \hat{\mathcal{H}}_S + \hat{\mathcal{H}}_p + \hat{\mathcal{H}}_{Sp} \tag{2}$$

The first new term $\hat{\mathcal{H}}_p = \hbar\omega_r(t)(1/2 + a^\dagger a)$ represents the photon field of variable frequency $\omega_r(t) = \omega_0 + \delta(t)$, where $a^\dagger$ and a are the creation/annihilation operators that satisfy $[a^\dagger, a] = 1$. The last term $\hat{\mathcal{H}}_{Sp}$ models the interaction between a N-spin ensemble and a MW photon. It can be expressed by the Holstein-Primarkoff transformation

$$\begin{aligned}\hat{\mathcal{H}}_{Sp} = \textstyle\sum_j \hbar G_j \left(e^{i\vartheta_j}\sigma_j^\dagger + h.c.\right)(a^\dagger + a) = \\ = \hbar G_N (b^\dagger + b)(a^\dagger + a)\end{aligned} \tag{3}$$

where G_j is the coupling to each individual spin and $b^\dagger$ the collective operator defined as

$$b^\dagger = \frac{1}{\sqrt{N\bar{G}^2}} \sum_j G_j e^{i\vartheta_j \sigma_j^\dagger} \;\; ; \;\; \bar{G}^2 \equiv \sum_j \frac{G_j^2}{2} \tag{4}$$

that also satisfies the bosonic relation $[b^\dagger, b] = 1$ in the low-polarization limit and $G_N = \sqrt{N\bar{G}^2}$ is the effective coupling constant.

Supposing that we are in weak coupling regime and close to a spin transition, the transmission of the resonator in the superconducting circuit can be modeled as

$$t = \left| 1 - e^{i\phi} \frac{A\kappa}{\kappa + i(f_{S,i} - f)} \right| \tag{5}$$

where A is the visibility of the resonator, $f_{S,i}$ is the frequency of the i-th resonant spin transition and κ is the effective resonator broadening, which depends on the intrinsic circuit line width κ_0 and on the resonant absorption of MW photons by the spin system. It can be written as

$$\kappa = \kappa_0 + \sum_i \frac{G_{N,i}^2 \gamma_i}{(g_{eff,i}\mu_B B_r - \omega_r)^2 + \gamma_i^2} \tag{6}$$

with $G_{N,i}$ the collective spin-photon coupling at each transition i, $g_{eff,i}$ its effective Landé factor and γ_i the spin global decoherence rate, which includes all the dissipating effects. It is related to the width of spin energy levels. For simplicity, we will consider $\gamma_i = \gamma = 1/T_2^*$.

After characterizing our hybrid system, the next step should be applying time-resolved MW pulses to a) measure the T_2 and characterize the spin coherence of our molecules and b) perform simple operations to test the viability of our proposal as a two-qubit system [17].

III. RESULTS

A. Spin-photon coupling for model $S = 1/2$ free radical molecules

In order to get a deeper understanding of all the concepts introduced previously, we are going to study first the simplest situation: a $S = 1/2$ organic free radical. This system can be achieved just by trapping a single electron in a molecule, a PTMr in this case (Fig. 2a). The spin Hamiltonian expressed in (1) gets reduced to just one electronic Zeeman interaction term

$$\hat{\mathcal{H}}_{S,PTMr} = -g\mu_B \vec{B} \cdot \vec{S} \tag{7}$$

where $g \approx 2$ is now isotropic. Moreover, using the rotational wave approximation, the spin-photon coupling term gets transformed to

$$\hat{\mathcal{H}}_{Sp,PTMr} = G_N(\hat{\sigma}^+\hat{a} + \hat{\sigma}^-\hat{a}^+) \tag{8}$$

with G_N the spin-photon coupling constant. It can be shown that the eigenvalues of the total Hamiltonian are then

$$E_n^{\pm} = \omega_r n + \frac{1}{2}(\delta \pm \sqrt{4G^2 n + \delta^2}) \tag{9}$$

where n is the number of MW photons and $\delta = g\mu_B B - \omega_r$ is the detuning between photon and spin excitations.

Using the equipment described in Section II A, we measured the line transmission at $T = 8$ mK and different power values. This very low-temperature regime allows us to associate the transmission dips with the resonant spin excitations. Figure 2b shows an example of the data collected, where we distinguish a central valley whose center evolves with B and even disappears for certain magnetic field values. This is related to the spin-photon coupling: when we increase B so that $\delta \to 0$, the difference between E_n^+ and E_n^- in (9) starts to grow, being the maximum at $\delta = 0$. In this case, both energies are associated with entangled light-matter states and their difference enable us to calculate G_N. Supposing $n = 1$ due to the low powers, we can estimate the coupling dependence with power.

This is represented in Figure 2c, where we can highlight two different aspects. The first one is the tendency to a constant value when the input power gets reduced. This

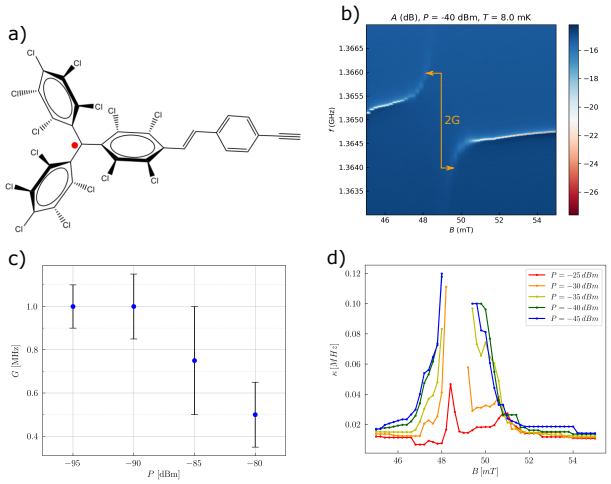

FIG. 2. a) Molecular structure of the PTMr molecule, where the red dot indicates the free radical. b) 2D plot of the line transmission measured at $T = 8$ mK and $P = -90$ dBm, with the magnetic field applied along the z axis. c) Dependence of the coupling constant G_N with the input signal power. d) Absorption spectra for different signal powers.

can be explained by the fact that we have supposed a low power regime ($n = 1$) and this holds true as long as we do not increase it to high values. This limit breaks down when $P \geq -85$ dBm, where we can suppose that $n > 1$, so the coupling constant G must decrease in order to fulfill $\Delta E_n^{\pm} = 2G\sqrt{n}$. However, for small powers, we can assume $G = (1.0 \pm 0.1)$ MHz. The second aspect is related to the uncertainty of the measures, which are quite big in because of the difficulty to resolve the beginning of each energy line.

If we focus on the transmission, knowing that it must follow (5), we can obtain κ in order to estimate the absorption of the spin system. The dependence of κ on B for different powers is plotted in Figure 2d, where the fit could not be done for values of field where the coupling becomes so high that the transmission disappears and the weak coupling approximation is no longer applicable. We observe that the absorption increases with lower powers, which is related to the saturation of the system: if we transport a reduced amount of photon through the transmission line, a bigger fraction of them will be absorbed by the system in order to get excited, because of the fact that the system can absorb a finite number of photons per time unit.

Assuming that the fitted points correspond to the weak coupling regime, we use (6) to estimate the coupling constant $G = (1.2 \pm 0.4)$ MHz, which agrees well with the results shown in Fig. 2c. The spin line width $\gamma = (12 \pm 9)$ MHz, which implies $T_2^* = (80 \pm 60)$ ns. The uncertainties are telling us that this method is not optimal to obtain the parameters, due to the initial supposition that we are working in weak regime. In the future, we shall apply a more general fitting method, one that is not based on the assumption of weak coupling.

B. Coupling of a DyLaDy single crystal to an LC superconducting resonator

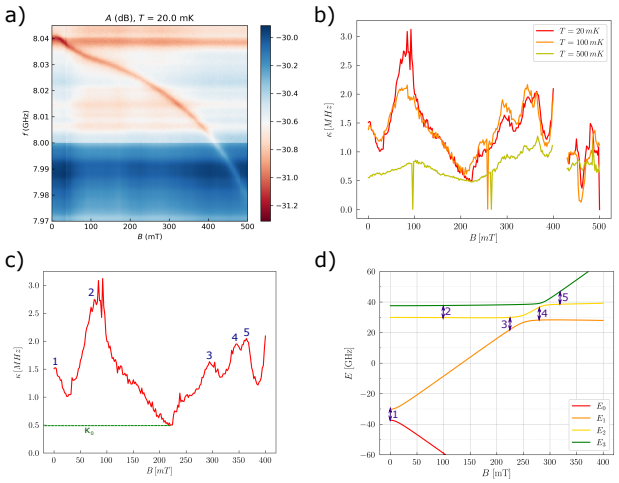

FIG. 3. a) 2D plot of the line transmission measured at $T = 20$ mK and $P = -70$ dBm, with the magnetic field applied along the z-axis. b) Absorption spectrum for different temperatures. c) Numeration of transitions in the $T = 20$ mK absorption spectrum. d) Energy level scheme with the location of the observed transitions.

Once we have seen the measurement and analysis procedures, we conduct the same experiment with the [DyLaDy] molecular trimer. The low visibility of this resonator required the application of a $P = -70$ dBm input power to resolve the resonance peaks from noise. We performed transmission measurements for three different temperatures, $T \in \{20, 100, 500\}$ mK, in order to discriminate spin absorption peaks arising from the ground or from excited states. An example of these measurements is shown in Figure 3a. We distinguish a transmission peak, characteristic of the LER resonance, whose central frequency decreases with B. Contrary to the PTM (Fig. 2b), this evolution is continuous, so we can guarantee that the spin-photon coupling remains within the weak regime at any B.

Fitting the data with (5), except in the range $B \in [400, 430]$ mT due to the change in the transmission given by the VNA, we obtain the absorption spectra shown in Figure 3b. This plot shows the influence of the temperature: the spin resonance peaks tend to be more intense for lower temperatures. This is because the population of the spin levels declines with the spin thermal agitation, which increases with the temperature, so there are less spins that can get excited by absorbing a photon.

Using the spectrum obtained at $T = 20$ mK because of its higher contrast, we can recognize several transitions, each of them associated with a peak in the absorption. Marked in Figure 3c, we can fit each one to (6) in order to obtain the coupling constant $G_{N,i}$, the effective Landé factor $g_{eff,i}$ and the spin global decoherence rate γ. In all cases, we got $\gamma = (5 \pm 0.2)$ GHz, which leads to $T_2^* = (0.2 \pm 0.008)$ ns, a very poor result for a qudit candidate. This large spin line width might be dominated by crystal imperfections, which give rise to multiple orientations of the spin anisotropy axes. Besides, $G_{N,i}$ and $g_{eff,i}$ depend on the transition, with values that are contained in $G_{N,i} \in [70, 110]$ MHz and $g_{eff,i} \in [1.9, 2.3]$.

The locations of the transitions can be used to estimate the $\tilde{g}_i$ tensors in (1). In first approximation, we can suppose that they are proportional to those found for the Er^{3+} ions (also with $J = 15/2$) in the analogous [ErCeEr] molecule [16]. Then, we can modify this degree of freedom in order to take the resonant transitions (given by $\Delta E = 8$ GHz, the main frequency of the photons) in the observed fields. The best fit is shown in Figure 3d, where we can only situate correctly the two first ones. This result indicates that the tensors of this molecules are not simply related to the ones in [ErCeEr], which can be explained by the influence of the presence/absence of the central magentic ion.

C. Spin dynamics with time-resolved pulses on free radical molecules

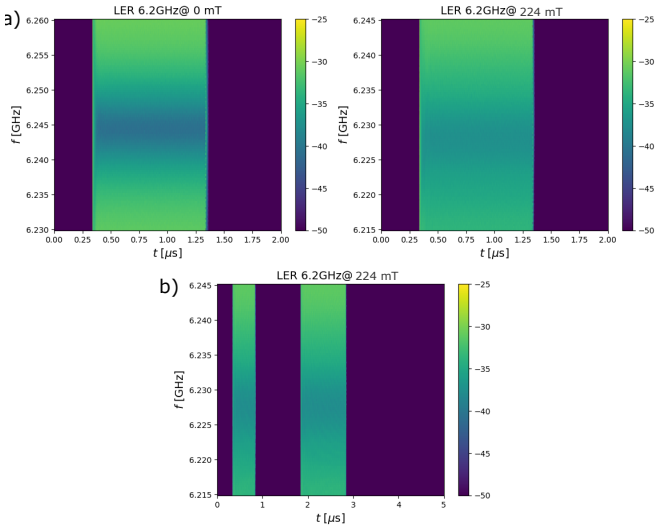

FIG. 4. a) 2D plots of the line transmission measured during the application and removal of a 1 μs long microwave pulse at $B = 0$ mT (left) and $B = 224$ mT (right). b) 2D plots of the line transmission measured during the two-pulse sequence at $B = 224$ mT.

We have already characterized the spin system in the stationary state of a $S = 1/2$ molecule and of our target molecule. The next step is then studying the spin dynamics in order to evaluate its viability as a qudit. With this aim, we start with the first molecule, the PTMr.

The first element to portray is the dynamics of the resonator charging and discharging, which depends on the photon life times. For this purpose, we measure the transmission during the application and removal of a 1 μs

long MW pulse using the QCS. Figure 4a shows a comparative at $B = 0$ mT, when there is no coupling with the spin system, and at $B = 224$ mT, when $\delta \longrightarrow 0$ for this resonator. In the stationary state, the spin-photon coupling leads to a shift in the resonator frequency and increases the resonator width. These results confirm those already measured with the VNA. However, here we see that the coupling also modifies the photon dynamics: for photons decoupled from the spins $t_l \approx 10$ ns, whereas t_l becomes much shorter, < 1 ns when the magentic field puts the spins in resonance with the circuit. This fast decay ensures that the spin echo signal does not get obscured by the signal associated by the photon decay, which is a desirable characteristic for these experiments.

Succeeding in this aspect, we attempt to perform a two-pulse sequence in order to measure the Hahn echo [17]. Choosing a 500 ns ($\frac{\pi}{2}$) pulse followed by a 1 μs (π) pulse separated by $\tau = 1\,\mu$s, it is expected to measure a signal after a time τ after the termination of the second pulse. Unfortunately, we had been unable to resolve the spin-echo signal yet, as can be seen in Figure 4b. Although this can be related to the number of excited spins, then with the intensity of the pulses, it is a problem we are currently working in.

IV. CONCLUSIONS AND OUTLOOK

In a general view, we have corroborated that superconducting circuits provide a good platform to interact with molecular spin qubits and qudits. For the first case, we have use a PTMr and we have seen that it has a strong coupling with the resonator, characterized by the splitting of the MW transmission lines. The dependence with input power has allowed us to estimate the spin-photon coupling constant in the single-photon limit. The evolution with magnetic field enabled us to determine the spin line width, which parameterizes the spin decoherence.

For our target molecule, the [DyLaDy] trimer, we have determined experimentally the presence of multiple spin resonances, arising from its more complex spin level spectrum. We find that the effective g-tensors differ from those previously found for an analogous [ErCeEr] molecular trimer, likely on account of the different nature of the Dy magnetic orbitals and the absence of a central magnetic ion. Additional experiments are planned in order to characterize it, such as electron paramagnetic resonance, heat capacity and magnetic susceptibility. Besides, we find that the spin line widths are quite large, pointing to the presence of sizable crystal defects. X-ray diffraction experiments will be performed in order to find out the structure of the sample used in these experiments.

Finally, we have started with pulse experiments on the model PTMr sample in order to set-up the conditions (chip design and pulse sequences) needed to control and detect its coherent spin dynamics. Although we have been able to characterize the photon life times in the bare resonator and in the coupling regime, getting promising results, we could not yet detect the Hahn echo after a two-pulse sequence due to the high noise to signal levels.

Further work will allow us to enlarge the SNR in the pulse experiments so as to resolve the echoes and to fully characterize our trimer and its spin global decoherence time constant, which will determine its viability as a qudit. If so, pulse experiments will be performed in it with the aim to find the optimal parameters for applying quantum gates.

[1] E. Gibney, "Physics: Quantum computer quest", *Nature* **516**, 24-26 (2014).

[2] P. W. Shor, "Polynomial-Time Algorithms for Prime Factorization and Discrete Logarithms on a Quantum Computer". *SIAM J. Comput.* **26** (5), 1484-1509 (1997).

[3] H. Liu, S. Nie, "Solving the 0-1 Knapsack Problem with Polynomial-Time Quantum Algorithm", *CCIS* **289**, 377-384 (2012).

[4] E. Knill, R. Laflamme, "Theory of quantum error-correcting codes", *Phys. Rev. A.* **55**, 900-911 (1997).

[5] J. Preskill, "Quantum computing in the NISQ era and beyond", *Quantum* **2**, 79 (2018).

[6] D. Loss, D. P. DiVincenzo, "Quantum computation with quantum dots", *Phys. Rev. A.* **57**, 120-126 (1998).

[7] J. J. Pla et al., "A single-atom electron spin qubit in silicon", *Nature* **489**, 541-545 (2012).

[8] A. Gaita-Ariño et al., "Molecular spins for quantum computation", *Nat. Chem.* **11**, 301-309 (2016).

[9] S. Carretta et al., "A perspective on scaling up quantum computation with molecular spins", *Appl. Phys. Lett.* **118**, 240501 (2021).

[10] J. M. Zadrozny et al., "Millisecond coherence time in a tunable molecular electronic spin qubit", *ACS Cent. Sci.* **1**, 488-492 (2015).

[11] M. Jenkins et al., "Coupling single-molecule magnets to quantum circuits", *New Journal of Physics* **15**, 095007 (2013).

[12] R. J. Schoelkopf, S. M. Girvin, "Wiring up quantum systems", *Nature* **451**, 664-669 (2008).

[13] M. D. Jenkins et al., "A scalable architecture for quantum computation with molecular nanomagnets", *Dalton Trans.* **45**, 16682-16693 (2016).

[14] A. Chiesa et al., "Blueprint for a Molecular-Spin Quantum Processor", *Phys. Rev. A.* **19**, 064060 (2023).

[15] D. Aguilà et al., "Heterodimetallic [LnLn'] Lanthanide Complexes: Toward a Chemical Design of Two-Qubit Molecular Spin Quantum Gates", *J. Am. Chem. Soc.* **136**, 14215-14222 (2014).

[16] E. Macaluso et al., "A heterometallic [LnLn'Ln] lanthanide complex as a qubit with embedded quantum error correction", *Chem. Sci.* **11**, 10337-10343 (2020).

[17] Stoll, S., *Pulse EPR* in *EPR Spectroscopy: Fundamentals and Methods*, 215-233. John Wiley & Sons (2018).